Eur. Phys. J. D **18**, 327–333 (2002)
DOI: 10.1140/epjd/e20020037

THE EUROPEAN PHYSICAL JOURNAL D
EDP Sciences

Density functional calculations for shell closures in Mg clusters

Ll. Serra[1,a], P.-G. Reinhard[2], and E. Suraud[3]

[1] Departament de Física, Universitat de les Illes Balears, 07071 Palma de Mallorca, Spain
[2] Institut für Theoretische Physik, Universität Erlangen, Staudtstrasse 7, 91058 Erlangen, Germany
[3] Laboratoire de Physique Quantique, Université Paul Sabatier, 118 route de Narbonne, 31062 Toulouse Cedex, France

Received 3 July 2001 and Received in final form 29 October 2001

Abstract. Motivated by recent measurements on Mg clusters we discuss the electronic structure and shell closures of these type of systems in the framework of self-consistent mean fields derived from density-functional theory. The ionic background is treated at different levels of refinement: spherical jellium model, and the spherically-averaged-pseudo-potential scheme (SAPS) with local as well as non-local pseudo-potentials. The ionic positions in SAPS are optimized using a Metropolis simulated annealing. It is shown that the details of ionic background influence sensitively the electronic levels sequence near the Fermi energy. In particular, the non-local effects from the pseudo-potential change the relations between states with high and with low angular momentum. Some of these effects go into the right direction towards experiment.

PACS. 31.70.-f Effects of atomic and molecular interactions on electronic structure – 36.40.Cg Electronic and magnetic properties of clusters

1 Introduction

The appearance of magic numbers due to electronic shell closures is a key feature in the physics of metal clusters since its very beginnings [1]. A wealth of studies have been devoted to that effect, particularly for monovalent simple metals — for reviews see [2,3]. The typical sequence of magic shell closures for Na clusters is for electron numbers $N_{\rm el}$ = 8, 20, 40, 58, and 92 with a hint of sub-shell closure at 34. Just recently, new experimental information has shown up on shell closures in Mg clusters [4]. Peaks in the abundances indicate shell closures at $N_{\rm el}$ = 20, 40, 60, 70, 80, and 94. The results are surprising because they deviate from the magic sequences which had been obtained from monovalent simple metals and because they cannot be reproduced easily with the simple jellium models which had been successful previously. The experimental paper [4] proposes an interpretation with a spherical shell model where high angular momentum states are better bound and dive through their companion states with lower l. It is the aim of this paper to discuss these experimental findings from a theoretical perspective. We want to explore the possibilities of a description in terms of spherical mean fields. We minimize arbitrariness by considering only self-consistent mean fields in the framework of density functional theory.

The theoretical description of electronic shell closures in metal clusters has a long history. The gross trends are already very well reproduced by the simple jellium model [5]. This first version used a steep fall off for the jellium density distribution. A softened surface transition yields more realistic results for several observables [6]. It does also influence the sequence of shell closures for large clusters [7]. But the *ad hoc* modeling within the jellium model quickly introduces too many free parameters. An unambiguous approach is provided by the use of pseudo-potentials in the context of density-functional theory. For metals, it suffices to restrict considerations to the valence electrons only and to use then pseudo-potentials for the interaction between valence electrons and ions. The necessary density functionals and pseudo-potentials are developed independently using information from the electron gas, from bulk material and from atoms. The approach thus contains no free parameters any more. There exist already several fully fledged density-functional calculations for Mg clusters [8–10]. These are, however, extremely demanding and thus limited to small systems going up to N = 13 in [8,9] and showing Mg_{35} in [10]. In order to extend such parameter-free approaches to larger systems, symmetry restricted methods have been developed. Most efficient is the spherically averaged pseudo-potential scheme (SAPS) which deals with detailed ions in full three-dimensional space but uses spherically averaged mean-fields for the interaction with the electrons [11].

[a] e-mail: dfslsc4@clust.uib.es

This scheme was also very successful in reproducing the magic shells observed for monovalent simple metals [12].

In its initial formulation the pseudo-potentials that entered the SAPS model were of a local type, partly because of their simpler structure and, also, because for simple metals it is known that non-local effects are rather small. Nevertheless, further refinements of the theoretical models necessarily require the use of realistic electron-ion interactions of a non-local nature. Extensions of the jellium model to account for non-local effects in Li clusters have been presented in references [13–15]. It is the aim of this paper to study the shell closures in Mg clusters using SAPS. This limits, of course, considerations to spherical systems. But this restriction is no hindrance for the present study because we are anyway after spherical shell closures. In addition, we shall use both local and non-local pseudo-potentials, in order to assess the relevance of the latter for Mg clusters.

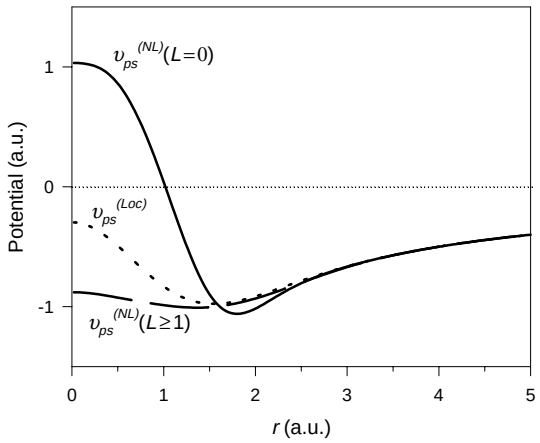

Fig. 1. Atomic pseudo-potentials of Bachelet, Hamann and Schlüter [18], $v_{\rm ps}^{(\rm NL)}$, for different angular momenta L. Also shown is the local approximation $v_{\rm ps}^{(\rm Loc)}$ mentioned in the text.

2 Formal framework

Within the SAPS model the external field on the valence electrons is obtained by spherically averaging the contribution from each ion. This reads, *e.g.*, for a local pseudo-potential

$$V_{\rm ext}(r) = \sum_{i=1}^{N_{\rm ion}} \frac{1}{4\pi} \int {\rm d}\Omega_i \, v_{\rm ps}^{(i)} \left(|\mathbf{r} - \mathbf{R}_i|\right), \qquad (1)$$

where $v_{\rm ps}^{(i)}$ corresponds to the ion at position $\mathbf{R}_i$ and ${\rm d}\Omega_i$ is the angular element of $\mathbf{R}_i$. The more involved case of non-local pseudo-potentials is discussed in [15]. At first sight this might seem a rather crude approximation. However it becomes more sensible when realizing that for certain ionic distributions a sum over ions actually implies an approximate spherical average as happens, of course, when ions arrange themselves in nearly radial shells. The imposed rotational invariance allows us to separate the angular parts $Y_{\ell m}(\theta, \phi)$ of the single electron wave functions and to remain with an effective one-dimensional problem (the radial equation) for the radial parts $R_{n\ell}(r)$.

In the literature there exist different kinds of pseudo-potentials that could be used in equation (1); see, *e.g.*, references [16–18]. The most refined are the non-local ones whose quality is guaranteed by the properties of orthogonalization to core states and norm conservation of the corresponding pseudo-wavefunctions with respect to the exact ones. Another important issue is the transferability of the pseudo-wavefunctions, which assures that their radial slopes at the core radius are correctly reproduced and, therefore, they can be used in different chemical environments. In this work we shall use the pseudo-potentials developed by Bachelet, Hamann and Schlüter which, by construction, fulfill all these properties [18].

Ab initio pseudo-potentials, such as those of reference [18], are by construction non-local because the deeplying shells are simply projected out. One can often develop simpler potentials if one is not interested on the details of the electronic wavefunction near the ionic cores. Particularly simple metals often allow to deal with purely local pseudo-potentials. A typical example is the always friendly Na (while a counterexample is its close relative Li) [13–15]. Thus we want to check the features of the Mg clusters when employing a local pseudo-potential. Once a local description is found to be sufficient, one could derive the necessary properties of a jellium model for that case. There is no local pseudo-potential for Mg readily available in the literature. We thus have developed a new pseudo-potential following the strategy of [19]. We employ a soft shape in terms of error functions (in atomic units),

$$v_{\rm ps}^{\rm Loc}(\mathbf{r} - \mathbf{R}_I) = \sum_{i=1,2} c_i \, \frac{{\rm erf}\left(|(\mathbf{r} - \mathbf{R}_I)|/\sqrt{2}\sigma_i\right)}{|\boldsymbol{r} - \boldsymbol{R}|}, \qquad (2)$$

where ${\rm erf}(r) = \int_0^r {\rm d}r' \, \exp\left(-r'^2/2\sigma_i^2\right)$. A boundary condition is $c_1 + c_2 = 1$. There remain three parameters, c_2, σ_1 and σ_2. The fitting strategy is similar as in [19]. We adjust the parameters to reproduce basic properties of the Mg atom (ground state energy and first excited state) and of the bulk (Wigner-Seitz radius $r_{\rm s} = 2.66\, a_0$). Fitting the two extremes of atom and bulk delivers fair properties for systems of intermediate size. We find the parameters $\sigma_1 = 0.42466\, a_0$, $\sigma_2 = 0.84932\, a_0$, and $c_2 = 3$. The spherical averaging of that simple form is straightforward. We skip the details here and will only show in Figure 1 the radial dependence of the local $v_{\rm ps}^{(\rm Loc)}$ and non-local $v_{\rm ps}^{(\rm NL)}$ pseudo-potentials (the latter depending on the multipolarity L of the atomic electron). We notice that the non-local pseudo-potential is strongly repulsive in the core region for s electrons and attractive for $L \geq 1$. The local approximation obviously amounts to a compromise between the two rather different behaviors for $L = 1$ and $L \geq 1$.

Having determined the external potential to be used the remaining electronic contributions are described within the local-spin-density approximation (LSDA) to density functional theory. This approach has been extensively used to describe a variety of non-uniform electronic

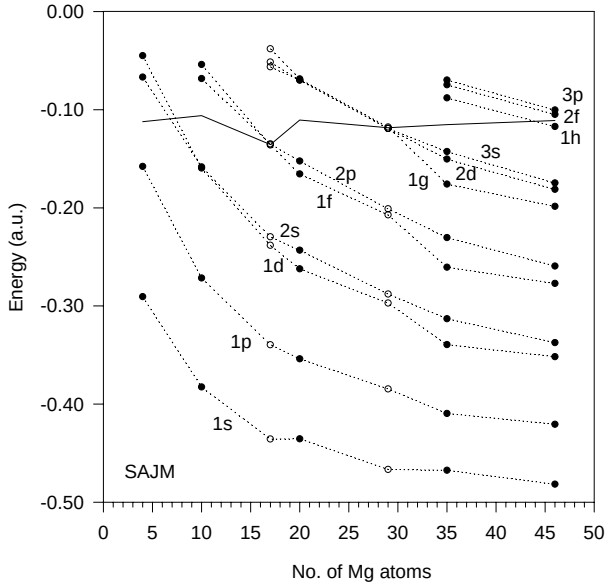

Fig. 2. Single electron spectra for spherical Mg clusters computed in the SAJM for Wigner-Seitz radius $r_s = 2.66\,a_0$ and subsequent Ashcroft core radius $r_c = 1.33\,a_0$ [23]. Occupied and unoccupied levels for each size are separated by the solid line, which corresponds to $(\varepsilon_{\rm HOMO} + \varepsilon_{\rm LUMO})/2$. Open shell configurations are indicated by open circles.

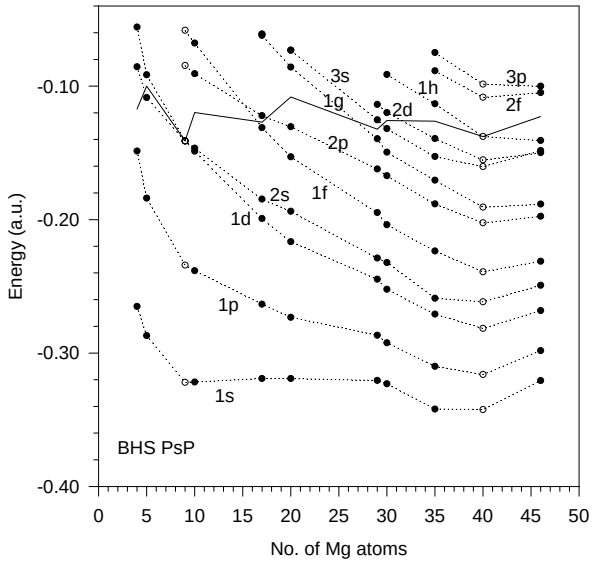

Fig. 3. Same as Figure 2 for spherical Mg clusters computed in SAPS with the non-local pseudo-potential of Bachelet, Hamann and Schlüter (BHS-PsP) [18].

systems and we shall refer the reader to reference [3] for a review on its use in the context of cluster physics. It is worth to mention, nevertheless, that we have employed the parameterization by Perdew and Zunger [20] of the exact Monte Carlo results for the bulk gas obtained by Ceperley and Alder [21].

The ionic positions in the ground state of a given cluster have been determined by a simulated annealing with the Metropolis algorithm (see, *e.g.*, Ref. [22]). This scheme implies an efficient exploration of the configuration space in the process of total energy minimization. Besides the standard electron-electron terms, the total energy contains the ion-electron $E_{\rm ie}$ and ion-ion $E_{\rm ii}$ energies. The former is given in terms of the electronic orbitals φ_i and external field as

$$E_{\rm ie} = \sum_{i=1}^{N_{\rm el}} \langle \varphi_i | V_{\rm ext} | \varphi_i \rangle \ , \tag{3}$$

while the ion-ion contribution to the total energy can be obtained from the classical expression for point charges

$$E_{\rm ii} = \sum_{i>j}^{N_{\rm ion}} \frac{Z_{\rm v}^2}{|\mathbf{R}_i - \mathbf{R}_j|} \tag{4}$$

where $Z_{\rm v}$ is the ionic valence.

3 Results and discussion

3.1 A preview in the jellium model

The first level of approach is the jellium model. From the various options we consider here the structure averaged jellium model (SAJM) which determines the softness of the jellium surface from local pseudo-potentials and which contains global information on the underlying ionic structure [23]. Figure 2 shows the single electron spectra for the expected spherical clusters. We remind the reader that only the valence electron orbitals are considered. They extend over the whole cluster and can be sorted with the standard atomic notation (*e.g.*, "1s" for the lowest state with angular momentum $l=0$). We read off from Figure 2 the sequence of magic shell closures $N_{\rm el} = 8$, 20, 40, 70. The $N_{\rm el} = 8$ is not supported by experiment. It seems that ionic structure effects and/or lack of metallicity prevails for this small cluster. The shells $N_{\rm el} = 20$, 40, and 70 come out as found in experiment. The SAJM thus reproduces correctly the loss of the $N_{\rm el} = 58$ shell (which was well developed in Na clusters) in favor of the 70. But it fails to reproduce the experimental $N_{\rm el} = 60$, 80 and 94 shell closures.

3.2 Local versus non-local pseudo-potentials

In order to explore the capabilities of a spherical description, we proceed to the most consistent treatment as given by SAPS. We have computed the structure of several Mg clusters up to $N_{\rm ion} = 46$ using SAPS with the non-local pseudo-potential of reference [18] and alternatively with a local pseudo-potential of the form as given in [19] and parameters especially adjusted to the case of Mg, see previous section. Only those clusters with an electronic shell closure at the level of SAPS are considered. The results with non-local pseudo-potentials are shown in Figure 3.

As is the SAJM the shell sequence resembles at first glance the spectrum in a spherical square well potential (*i.e.*, 1s, 1p, 1d, 2s, ...). We thus observe in the first stages the standard sequence of magic numbers, (2), 8, 20, 34, 40,

as it is well-known from monovalent simple metals [1–3]. A new feature amongst small clusters is the appearance of a magic $N_{\rm el}=10$ sub-shell closure. Systematic changes come up for larger clusters. We see the shell at $N_{\rm el}=58$ which is standard in Na clusters and which was absent in the SAJM for Mg is identifiable here, but it is degraded and a new shell closure follows immediately at $N_{\rm el}=60$. The $N_{\rm el}=70$ shell which was already found in the SAJM persists while the $N_{\rm el}=92$, well-known from Na clusters but absent in SAJM and experiment, is enhanced. In the experiment this latter shell occurs at $N_{\rm el}=94$ instead of 92.

We have compared the spectra of Figure 3 with those of previous full 3D calculations. For the small clusters, we find very good agreement for Mg_{10} and acceptable results for Mg_5 and Mg_4 [9]. Our spectrum for Mg_{35} agrees surprisingly well with that from [10] although the ionic shape is more spherical in SAPS.

A question is now to what extent the non-localities of the pseudo-potential play a role. To answer this question, we have performed similar SAPS calculations with a purely local pseudo-potential. The results are shown in Figure 4. At first glance, they look much similar. More detailed inspection, however, shows interesting differences in the relations between neighboring shells. There is a marked difference already for the small $N_{\rm el}=10$ cluster. It is magic for the non-local pseudo-potential (see previous figure) and non-magic here. The non-locality manifests especially in the cluster s states, adding an extra piece of attraction. Such an extra bit makes a large effect in cases of near degeneracy. A similar effect is seen in the $1g$–$2d$–$3s$ shell where the downshift of the $3s$ state gives rise to the new shell closure at $N_{\rm el}=60$, not seen with the local potential. The extra attraction on the s states has an effect already for the small $N_{\rm el}=18$. We have a shell closure with the local potential which disappears completely with the non-local one.

An extra attraction from the non-local part also affects to some extent the subsequent low l states. Looking at the relation between the $1f$ and the $2p$ orbitals, we notice that the local potential produces a large gap between these two shells giving rise to a well developed magic $N_{\rm el}=34$. The non-local potential, however, drives the $2p$ state closer to the 1f state which almost wipes out that shell closure. The revival of the $N_{\rm el}=70$ is also seen with the local pseudo-potential but not as pronounced as with the non-local one. It is obviously a mix of effects, coming already from the different radius and surface properties, as compared to alkali clusters, and being enhanced by the non-locality. The case $N_{\rm el}=92$ is well magic in both approximations although non-locality also manifests in the level scheme. In particular we notice that the HOMO level is $1h$ in non-local SAPS, while for the local approach it is $3s$ due to its less binding. It is to be remarked that the $N_{\rm el}=92$ shell was absent in the SAJM, see Figure 2, thus showing the importance of ionic structure versus a smoothened background.

Comparing the last three figures, we see an interesting difference between the SAPS results, Figures 3 and 4, and

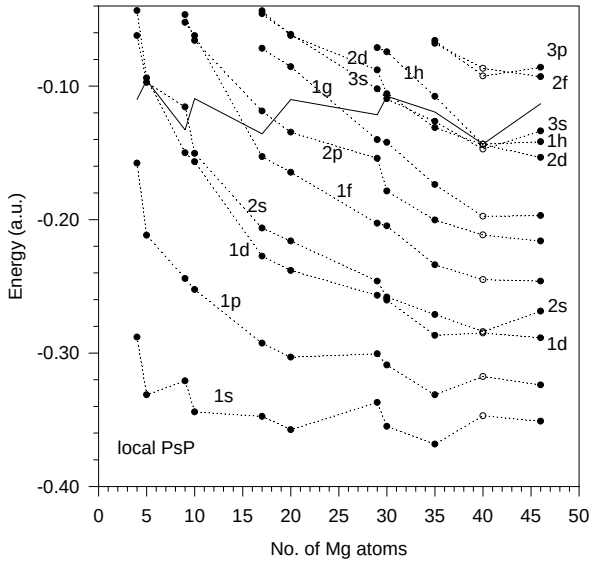

Fig. 4. Same as Figure 2 with the local pseudo-potential as described in Section 2.

the SAJM, Figure 2. Although the level schemes within one given cluster are generally similar, the SAPS results show more fluctuations in the trends *versus* system size due to the combined electronic and ionic structures. This is particularly pronounced for the step to Mg_{46}. It is to be noted that our calculations are done practically at zero temperature. Thus we see here most probably an effect of ionic structure, which is of course absent in the SAJM.

Finally, it is interesting to test to what extent a possibly positive net charge of the clusters would affect the results. We have checked that for a doubly charged Mg_{36}^{++} in comparison with the neutral Mg_{35}, both having the same $N_{\rm el}=70$. The overall binding is of course increased, but the relative level ordering remains unchanged. The results concerning electronic shell closures are thus robust.

3.3 A first summary

We now give a brief summary of the findings from Figures 2, 3, and 4 corresponding to SAJM, SAPS with non-local pseudo-potentials, and local SAPS. All three models predict the low shell closures 2, 8, 20, and 40. The smallest, 2 and 8, are not seen experimentally, probably because metallicity has not yet been well developed. The non-local SAPS produces also a magic $N_{\rm el}=10$. This hints already that local *versus* non-local effects can play a crucial role in determining the details of shell closures. Similarly, there is a visible difference between local and non-local SAPS concerning the sub-shell closure at $N_{\rm el}=10$. Larger differences develop for larger clusters. The SAJM has no $N_{\rm el}=58$ shell (here in accordance with data) while both SAPS models show it more or less. Only the non-local SAPS produces a $N_{\rm el}=60$ shell as seen in experiment. All models agree on producing the $N_{\rm el}=70$ in accordance with data. The leading mechanism here is simply the smaller Wigner-Seitz radius ($r_{\rm s}=2.66\,a_0$) as compared to Na clusters ($r_{\rm s}=4\,a_0$).

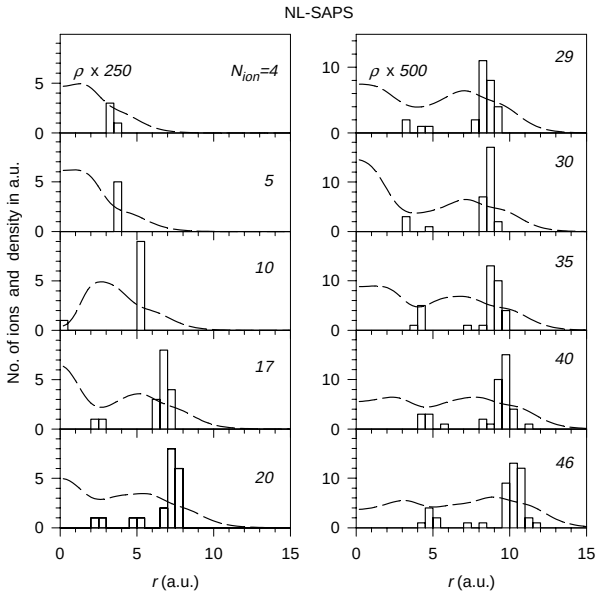

Fig. 5. Radial distribution of electrons (dashed line) and ions (collected in radial bins) for the set of spherical Mg clusters computed with SAPS using the the non-local pseudo-potential of [18].

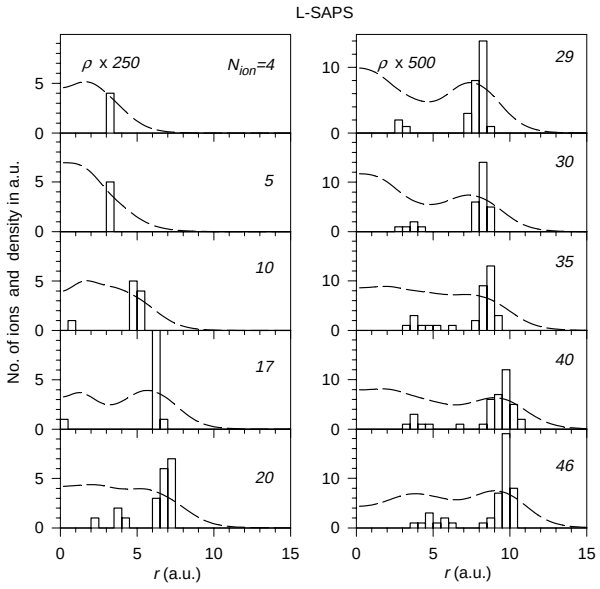

Fig. 6. Same as Figure 5 using the the local pseudo-potential as described in Section 2.

All spherical models fail to find the experimental $N_{\rm el}=94$ shell. There is a $N_{\rm el}=92$ shell in both SAPS while the SAJM has no shell closure in that region. The difference between the models is here driven by ionic structure effects.

Altogether, these examples have also shown that non-localities can induce differences in the sequence of magic shell closures. This effect is very pronounced for the example of Mg and has never been observed so distinctively for the monovalent simple metals as, *e.g.*, Na or K. From a theoretical point of view, the non-local SAPS is the most consistent of the spherical models. In practice, it produces the sequence $N_{\rm el}=(8)$, 10, 20, (34), 40, (58), 60, 70, and (92), which is only in partial agreement with experiment. The numbers in brackets are not found in experiment (also weak closures in theory) and the experimental 80 and 94 seem out of the scope of any one of the present models. This could be a deficiency of the spherical averaging over ionic structure or due to the occurrence of massively deformed shell closures. This has yet to be checked with symmetry unrestricted structure optimization which is very hard to do for such large clusters.

3.4 More details

For complementing the analysis it is interesting to look briefly at the spatial distribution of electrons and ions. The electrons are presented simply in terms of the radial density distribution $\rho(r)$. The ions are given in terms of detailed positions $\{\mathbf{R}_n, n=1,...,N_{\rm ion}\}$. The key feature in SAPS is their distance $R_n = |\mathbf{R}_n|$ from the center. We collect that in radial bins to produce a distribution which can be compared with the electronic density. The results for the non-local SAPS are shown in Figure 5. The ions arrange nicely in radial shells, one shell for the smaller and two shells for the larger clusters shown here. The electronic densities hint also radial shells which develop in parallel to the ionic shells. But it seems as if the electronic maxima rather avoid the ionic shells. The same figure for the local SAPS is shown in Figure 6. The ionic shells look much similar as before. But now the electronic maxima follow more closely the ionic shells. The comparison thus demonstrates the spatial repulsion of electrons out of the vicinity of the ionic cores. This difference in ion-electron interaction causes a visible difference of electronic distributions although the ionic distributions are very similar.

A closer look at the differences between local and non-local potentials is taken in Figure 7 for Mg_{30}, a case in which the non-local pseudo-potential delivers electronic shell closure while the local one does not. For better comparison, and in order to eliminate biases linked to slight differences in the ionic structures obtained with local and non-local pseudo-potentials, we consider one and the same ionic configuration in both cases and take that from the non-local model. The electronic densities agree globally. But note again the slight reduction of $\rho_{\rm NL}$ around the ionic positions. That is due to the projection of the $1s$ state in the non-local pseudo-potential. A complementing comparison of the single electron spectra is shown in the lower panel of Figure 7. The deep lying levels are similar. But there is a marked difference for the three levels around the Fermi surface. This group is almost degenerate for the local potential causing Mg_{30} to be non-magic while leaving a large magic gap for Mg_{29}. This test case with fixed ion configuration thus demonstrates that the strong effect on the single electron spectra is exclusively due to the non-locality of the pseudo-potential and not to an ionic effect.

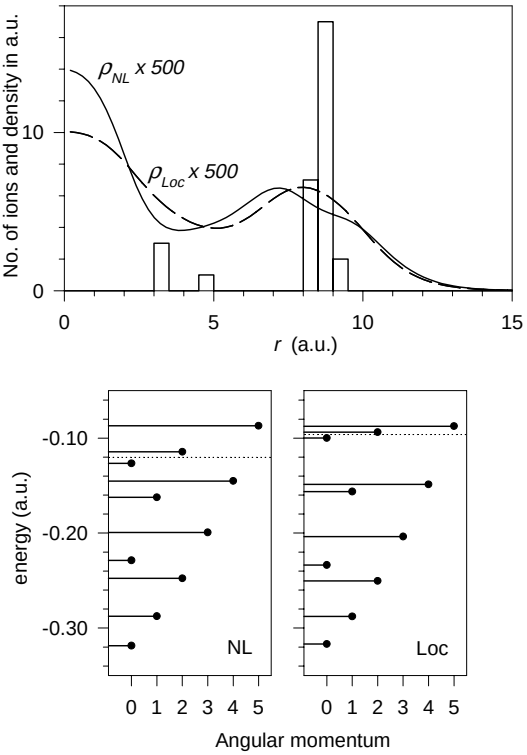

Fig. 7. Comparison of non-local (NL) and local (Loc) results for a fixed ionic distribution corresponding to Mg_{30}. Upper panel shows the electronic densities while lower ones display the energy level schemes. The dashed line denotes the Fermi energy.

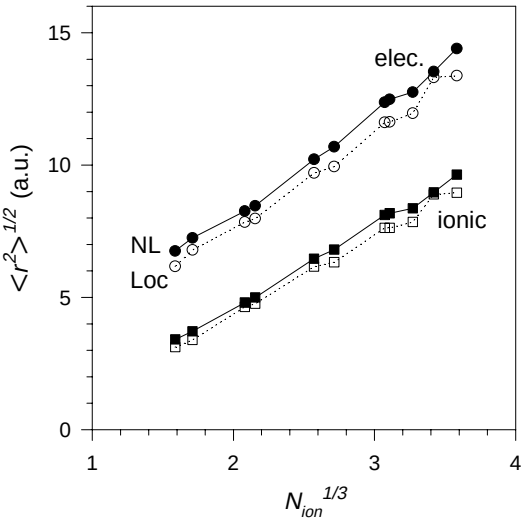

Fig. 8. Ionic and electronic root-mean-square radii of Mg clusters within the SAPS model. Circles and squares correspond to electronic and ionic distributions, respectively. Solid and open symbols indicate the non-local and local results, respectively.

Figure 8 finally compares the global geometries of the "local" and "non-local" clusters in terms of electronic and ionic r.m.s. radii. The ionic radii stay very close to each other. The electrons show slightly more differences where the radii are generally larger for the non-local case. This is a side-effect of the suppression of density near the ionic centers (see the preceding figure). Nonetheless, the differences in global properties are small throughout. It is just the more detailed single electron structure which reacts more sensitively to non-localities.

4 Conclusions

The electronic shell closures of Mg clusters with $N_{\rm ion} < 50$ have been investigated within density functional and *ab initio* pseudo-potential theory. We concentrated on spherical systems and used a spherical jellium model as well as a spherically averaged pseudo-potential scheme (SAPS) with Monte-Carlo optimization of ionic structure. A non-local *ab initio* pseudo-potential is used and alternatively also a local pseudo-potential in order to assess clearly the effects of non-locality. There are sizeable effects from non-locality and from ionic structure. The electronic density at ionic positions is reduced by projection. More importantly, there is a re-shuffling of electronic levels near the Fermi surface which has strong impact on the sequence of magic shell closures. Besides the standard shell closures for $N_{\rm el} = 8$, 20, 40, 58 and 92 we have also found enhanced closures at 34, 60 and 70. These findings are in partial agreement with experimental evidence. The $N_{\rm el} = 34$, 58 and 92 are not seen in the data while theory misses the pronounced experimental $N_{\rm el} = 80$ and 94 shells. It could be a deformed shell effect or a three-dimensional structural effect which both are invisible in SAPS. This case needs yet further investigation.

This work was supported in part by Grant No. PB98-0124 from DGESeIC, Spain. Two of the authors (P.-G.R. and E.S.) thank French-German exchange program PROCOPE numbers 95073 and 99074 and Institut universitaire de France for financial support.

References

1. W.D. Knight, K. Clemenger, W.A. de Heer, W.A. Saunders, M.Y. Chou, M.L. Cohen, Phys. Rev. Lett. **52**, 2141 (1984).
2. W.A. de Heer, Rev. Mod. Phys. **65**, 611 (1993).
3. M. Brack, Rev. Mod. Phys. **65**, 677 (1993).
4. T. Diederich, T. Döppner, J. Braune, J. Tiggesbäumker, K.-H. Meiwes-Broer, Phys. Rev. Lett. **86**, 4807 (2001).
5. W. Ekardt, Phys. Rev. Lett. **52**, 1925 (1984).
6. A. Rubio, L.C. Balbás, J.A. Alonso, Z. Phys. D **19**, 93 (1991)
7. J. Lermé, M. Pellarin, J.L. Vialle, M. Broyer, Phys. Rev. B **52**, 2868 (1995).
8. V. de Coulon, P. Delaly, P. Ballone, J. Buttet, F. Reuse, Z. Phys. D **19**, 173 (1991).
9. V. Kumar, R. Car, Phys. Rev. B **44**, 8243 (1991).

10. S.M. Reimann, M. Koskinnen, H. Häkinnen, P.E. Lindelof, M. Manninen, Phys. Rev. B **56**, 12147 (1997).
11. M.P. Iñiguez, M.J. López, J.A. Alonso, J.M. Soler, Z. Phys. D **11**, 163 (1989).
12. M.J. López, M.P. Iñiguez, J.A. Alonso, Phys. Rev. B **41**, 5636 (1990); M.J. López, A. Mañanes, J.A. Alonso, M.P. Iñiguez, Z. Phys. D **12**, 237 (1989); A. Mañanes, M.P. Iñiguez, M.J. López, J.A. Alonso, Phys. Rev. B **42**, 5000 (1990).
13. S.A. Blundell, C. Guet, Z. Phys. D **28**, 81 (1993).
14. K. Yabana, G.F. Bertsch, Phys. Rev. B **54**, 4484 (1996).
15. F. Alasia, Ll. Serra, R.A. Broglia, N. van Giai, E. Lipparini, H.E. Roman, Phys. Rev. B **52**, 8488 (1995).
16. N.W. Ashcroft, Phys. Lett. **23**, 48 (1966).
17. D.R. Hamann, M. Schlüter, C. Chiang, Phys. Rev. Lett. **43**, 1494 (1979).
18. G.B. Bachelet, D.R. Hamann, M. Schlüter, Phys. Rev. B **26**, 4199 (1982).
19. S. Kümmel, M. Brack, P.-G. Reinhard, Eur. Phys. J. D **9**, 149 (1999).
20. J.P. Perdew, A. Zunger, Phys. Rev. B **23**, 5048 (1981).
21. D.M. Ceperley, B.J. Alder, Phys. Rev. Lett. **45**, 566 (1980).
22. C. Kohl, F. Calvayrac, P.-G. Reinhard, E. Suraud, Surf. Sci. **405**, 74 (1998); C. Kohl, Ph.D. thesis, Erlangen, 1997.
23. B. Montag, P.-G. Reinhard, J. Meyer, Z. Phys. D **32**, 125 (1994).